Analog analysis of π-mode structures: Results and implications

Stan O. Schriber
Los Alamos National Laboratory, P.O. Box 1663, MS H820, Los Alamos, New Mexico 87545
(Received 29 June 2001; published 5 December 2001)

The cavities of choice for high-energy synchrotrons and for medium-beta and high-beta accelerating superconducting structures around the world are π-mode structures. A coupled-circuit analysis, allowing for errors in cell frequencies and cell coupling constants, has been used to determine relative on-axis electric field amplitudes between cells, operating frequencies, end-cell tuning, relative on-axis field phase shifts, and field tilts when operated off resonance. Formulas are given for the above information as well as specific examples showing sensitivities and machining/assembly/control tolerances. A method to determine relative field amplitudes on the basis of the mode spectra was developed.

DOI: 10.1103/PhysRevSTAB.4.122001 PACS numbers: 41.20.Jb, 84.40.-x, 02.60.Cb

I. *RLC* LOOP COUPLED CIRCUIT

Many of the rf cavities employed in high-energy synchrotrons and in superconducting accelerators use π-mode structures. Relative on-axis average electric field amplitudes between cells of a multicell cavity can be investigated using coupled-circuit analysis. This analysis method has been used effectively for many years, beginning with work by Dunn *et al.* [1–4] and carried on later at Los Alamos [5,6] and at Chalk River [7]. The later studies focused on $\pi/2$-mode cavities with their inherent stability properties. The work by Dunn *et al.* was rudimentary and showed simple aspects of circuit theory. This paper provides significant details on π-mode cavities and implications for their operations. LOOPER [8], a program written in 1981 to analyze coupled circuits for resonance characteristics, was used to verify predictions from the analytic formulas given below and is available from the Los Alamos Code Group [9]. LOOPER was validated from multicell calculations using SUPERFISH [10]: agreement to at least three significant figures for relative average on-axis field amplitudes and quality factors, and to at least nine for resonant frequencies. LOOPER also provides information on phase shifts along a structure, match to the drive(s), and beam coupling effects.

Figure 1 shows a coupled-circuit analog of a coupled-cell cavity with first-neighbor coupling between the all-identical loops. Resonant frequency for a cell is represented by the loop $\omega_0 = \sqrt{1/2LC}$, cell quality factor by $Q = 2\omega_0 L/R$, cell-to-cell coupling by k (the mutual inductance), and cell average on-axis electric field amplitude by the loop current amplitude, i_n.

The dispersion relationship for the coupled system shown in Fig. 1 is $f = f_0/\sqrt{1 + k\cos\phi}$, the frequency region over which an infinite chain of cells with cell resonant frequency f_0 can oscillate for a particular mode distribution, such as the TM_{010}. Solutions for ϕ of a finite chain with N cells, and the loop current amplitudes for end terminations of either half-cell or full cell, are given in Table I.

Within dispersion curve nomenclature, modes with 0 and π phase values exist for half-cell termination, but not for full-cell termination. However, the last full-cell termination mode, $\varphi = \pi N/(N + 1)$, is the only mode with π phase shifts between each cell; hence the rationale for the term π-mode. Similarly, the first mode is the only mode with 0 phase shifts between all cells; hence 0-mode. All other modes have combinations of 0, $\pi/2$, and π phase shifts between cells. Unlike a half-cell terminated cavity, relative cell field amplitudes are not flat for the two end modes, $q = 1$ or N, of a full-cell terminated cavity.

For the most efficient conversion of input rf power to beam power, it is desirable to equalize the average on-axis electric field amplitudes of each cell in the cavity. Achievement of equal cell fields is known as having flat fields, i.e., $|i_1| = |i_2| = |i_3| = \cdots = |i_N|$. Therefore, it is important to understand relative cell fields and how they are impacted by cavity variables.

Relative loop current amplitudes (representing average on-axis relative electric field amplitudes) are obtained by solving a set of N coupled equations using finite difference techniques where the nth loop voltage using Kirchoff's Law is given by

$$\left[R + j\left(2\omega L - \frac{1}{\omega C}\right)\right] i_n + j\omega kL(i_{n+1} + i_{n-1}) = 0,$$

and the set of N equations has the form ($A = 1/2$ for half-cell and $A = 1$ for full-cell termination):

$$\begin{aligned} AKi_1 + ki_2 &= 0, \\ Ki_2 + ki_3 + ki_1 &= 0, \\ &\vdots \\ Ki_n + ki_{n+1} + ki_{n-1} &= 0, \\ &\vdots \\ Ki_{N-1} + ki_N + ki_{N-2} &= 0, \\ AKi_N + ki_{N-1} &= 0, \end{aligned} \tag{1}$$

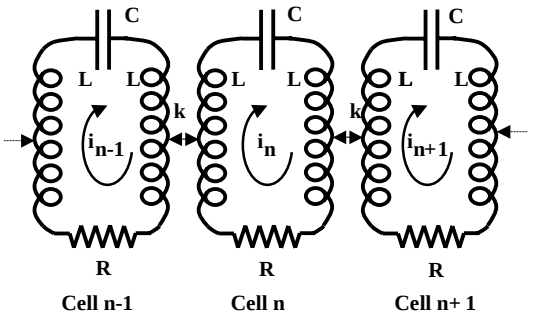

FIG. 1. *RLC* loop-coupled analog circuit for analyzing coupled accelerating cells.

with

$$K = 2\left[1 - \left(\frac{\omega_0}{\omega}\right)^2 - j\frac{\omega_0}{\omega Q}\right].$$

For flat fields in either the 0- or π-mode with full-cell termination, the first and last equations of Eq. (1) must be modified (to be similar to those for half-cell termination) by having end-cell frequencies given by $f_{\text{end}} = f_0\sqrt{(1 - gk/2)/(1 - gk)}$ with $g = 1$ for the π-mode and $g = -1$ for the 0-mode. However, when one of these modes at the end of the dispersion curve is made flat, the relative field distributions change for the rest of the modes, as does the dispersion curve for the chain. The π-mode frequency has an important correction factor α that accounts for Q, N and errors in the cavity defined by

$$f_\pi = \frac{f_0}{\sqrt{1 - k(1 + \alpha)}}. \tag{2}$$

In effect, the π-mode frequency correction factor α modifies the coupling constant from k to $k(1 + \alpha)$ in order to account for characteristics of a real cavity, not one that is errorless and/or lossless. The factor α can be positive or negative, has an absolute value less than 1 (usually less than 0.01), and is made up of two terms, α_0 (term accounting for finite Q and N) and α_{err} (term accounting for cell errors); $\alpha = \alpha_0 + \alpha_{\text{err}}$. The α_0 correction factor term is given by $\alpha_0 = 5(N - 1)(N - 1.5 + A)/8k^2Q^2$, where A is the termination constant defined earlier. This correction factor has been confirmed with LOOPER calculations of the π-mode frequency with error-free cavities to be accurate within nine significant figures for ks from 1% to 6%, cell numbers to nine, and loaded Qs as low as 10 000. The α_{err} term is determined by rearranging Eq. (2), yielding $\alpha_{\text{err}} = -1 + (1 - \{f_0/[f_\pi(\alpha_0) + df_\pi]\}^2)/k$, where $f_\pi(\alpha_0)$ is the errorless, corrected π-mode frequency and df_π is the frequency shift from cavity errors discussed in Sec. III B.

II. STEPWISE SOLUTIONS OF THE π-MODE EQUATIONS

Although it is possible to obtain solutions for a chain of coupled cells using analogs such as LOOPER, or from mesh codes such as SUPERFISH and/or MAFIA [11], it is worthwhile to understand the performance of a coupled system using analytic formulas that represent performance in an accurate manner. This can be particularly important for some characteristics of π-mode cavities. In addition, formulas give insight into system performance and the consequences of particular parameter changes. For these reasons, Eq. (1) was solved stepwise from the first equation to the last with drive e_N in cell N. This drive results in the last equation having the form $AKi_N + ki_{N-1} = e_N/j\omega L$, from which on-resonance (and off-resonance) characteristics with drive can be determined. A solution for i_2 in terms of i_1 is obtained from the first equation, a solution for i_3 in terms of i_1 is determined from the second equation using the i_2 solution, and so on until the second last equation from which i_N is determined. The last equation is used to solve for e_N in terms of i_1. Solutions presented below were found to agree with LOOPER calculations to within three significant figures for all cases studied. Differences in cell parameters (from assembly perturbations, errors, machining tolerances, etc.) are represented by different values for each cell: the nth cell frequency, $f_{0n} = f_0(1 + \Delta_n)$, and coupling between the nth and the $n + 1$th cell, $k_{n,n+1} = k(1 + \varepsilon_{n,n+1})$. The set of Eq. (1) becomes the following when cell differences are included:

TABLE I. Phase and loop amplitudes for half-cell and full-cell terminations.

End terminations	Phase value	Current amplitude	Mode numbering
Half cell	$\varphi = \frac{\pi(q - 1)}{N - 1}$	$i_n \propto \cos\frac{(n - 1)\pi(q - 1)}{N - 1}$	$q = 1, 2, 3, \ldots, N$
Full cell	$\varphi = \frac{\pi q}{N + 1}$	$i_n \propto \sin\frac{n\pi q}{N + 1}$	$q = 1, 2, 3, \ldots, N$

$$
\begin{aligned}
AK_1 i_1 + k(1 + \varepsilon_{1,2}) i_2 &= 0, \\
K_2 i_2 + k(1 + \varepsilon_{2,3}) i_3 + k(1 + \varepsilon_{1,2}) i_1 &= 0, \\
&\vdots \\
K_n i_n + k(1 + \varepsilon_{n,n+1}) i_{n+1} + k(1 + \varepsilon_{n-1,n}) i_{n-1} &= 0, \\
&\vdots \\
K_{N-1} i_{N-1} + k(1 + \varepsilon_{N-1,N}) i_N + k(1 + \varepsilon_{N-2,N-1}) i_{N-2} &= 0, \\
AK_N i_N + k(1 + \varepsilon_{N-1,N}) i_{N-1} &= e_N / j\omega L,
\end{aligned}
\tag{3}
$$

with

$$
K_n = 2k\left[1 + \alpha - \frac{2\Delta_n}{k} - j\left(\frac{1 + \Delta_n - \frac{k}{2}(1 + \alpha)}{kQ}\right)\right],
$$

except

$$
K_n = 2k\left[\frac{1}{2} + \alpha - \frac{2\Delta_n}{k} - j\left(\frac{1 + \Delta_n + \frac{k}{4} - \frac{k}{2}(1 + \alpha)}{kQ}\right)\right],
$$

for full-cell termination when $n = 1$ or N. Neglecting higher order terms gives the following complex solutions for the nth cell current amplitude in an N cell chain using a first cell amplitude of $i_1 = 1 + j0$:

$$
\begin{aligned}
i_n(\text{full})/(-1)^{n-1} \approx\ & 1 + n(n-1)\alpha - \frac{(n+1)n(n-1)(n-2)}{6k^2Q^2} \\
& \times \left[1 - k(1 + \alpha) + \frac{2(n-3)(n+2)\alpha}{15} + \frac{k}{(n+1)}\right] \\
& + \frac{\delta_1}{k^2Q^2} - \frac{4}{k}[(n-1)\Delta_1 + \cdots + 3\Delta_{n-3} + 2\Delta_{n-2} + \Delta_{n-1}] \\
& - (\cdots + 7\varepsilon_{n-4,n-3} + 5\varepsilon_{n-3,n-2} + 3\varepsilon_{n-2,n-1} + \varepsilon_{n-1,n}) \\
& - j\,\frac{n(n-1)}{kQ}\left[1 - \frac{k(1+\alpha)}{2} + \frac{(n-2)(n+1)\alpha}{3} + \frac{k}{2n} - \frac{\delta_2}{n(n-1)}\right].
\end{aligned}
\tag{4}
$$

As expected, a half-cell terminated cavity has similar relative amplitudes given by

$$
\begin{aligned}
i_n(\text{half})/(-1)^{n-1} \approx\ & 1 + (n-1)^2\alpha - \frac{n(n-1)^2(n-2)}{6k^2Q^2}\left[1 - k(1+\alpha) + \frac{2(n-3)(n+1)\alpha}{15}\right] + \frac{\delta_3}{k^2Q^2} \\
& - \frac{4}{k}\left[\frac{(n-1)}{2}\Delta_1 + \cdots + 3\Delta_{n-3} + 2\Delta_{n-2} + \Delta_{n-1}\right] \\
& - (\cdots + 7\varepsilon_{n-4,n-3} + 5\varepsilon_{n-3,n-2} + 3\varepsilon_{n-2,n-1} + \varepsilon_{n-1,n}) \\
& - j\,\frac{(n-1)^2}{kQ}\left[1 - \frac{k}{2}(1+\alpha) + \frac{n(n-2)\alpha}{3} - \frac{\delta_4}{(n-1)^2}\right].
\end{aligned}
\tag{5}
$$

Expected similarities are evident as is the importance of the π-mode frequency correction factor α. End-to-end field tilt depends on the fourth power of cell number to first order, and is linear to frequency and coupling constant errors. This fourth power dependence on N for field flatness is a powerful argument for choosing the number of cells in a cavity to be as small as reasonably possible. Also, because field tilt varies inversely to both the square of k and the square of Q, it is advantageous to have these two parameters as large as possible. In addition, a larger k results in the cavity being less sensitive to frequency errors. Note that full-cell termination has an extra k related term in both the real and the imaginary parts of the expression. Second order corrections, δ_1 to δ_4, to the above expressions are not needed unless errors are very large, and are included below for completeness with $\gamma = 1$ for $l = 1$ and $\gamma = 2$ for $l > 1$.

$$\delta_1 = \sum_{l=1}^{n-1}\left[\frac{2n(n-1)(n+1)(n-3)(n-2)}{15} - \sum_{m=2}^{l\geq m}\frac{2(n-2m)(n+1-2m)(n+2-2m)(n+3-2m)}{3}\right]\frac{\Delta_l}{k}$$
$$+ \sum_{l=1}^{n-1}\left[\frac{n(n-1)(2n^2-9n+29)(n-2)}{30} - \sum_{m=2}^{l\geq m}\frac{(n-1-2m)(n-2m)(n+1-2m)(n+2-2m)}{3}\right]\varepsilon_{l,l+1},$$

$$\delta_3 = \sum_{l=1}^{n-1}\left[\gamma\frac{n(n-1)(n+1)(n-3)(n-2)}{15} - \sum_{m=2}^{l\geq m}\frac{2(n+1-2m)(n+2-2m)^2(n+3-2m)}{3}\right]\frac{\Delta_l}{k}$$
$$+ \sum_{l=1}^{n-1}\left[\frac{n(n-1)(2n^2-9n+19)(n-2)}{30} - \sum_{m=2}^{l\geq m}\frac{(n-2m)(n+1-2m)^2(n+2-2m)}{3}\right]\varepsilon_{l,l+1},$$

$$\delta_2 = \sum_{l=1}^{n-1}\left[\frac{4n(n-1)(n-2)}{3} - \sum_{m=2}^{l\geq m}4(n+1-2m)(n+2-2m)\right]\frac{\Delta_l}{k}$$
$$+ \sum_{l=1}^{n-1}\left[\frac{(n-1)(2n^2-7n+12)}{3} - \sum_{m=2}^{l\geq m}2(n-2m)(n+1-2m)\right]\varepsilon_{l,l+1},$$

$$\delta_4 = \sum_{l=1}^{n-1}\left[\gamma\frac{2n(n-1)(n-2)}{3} - \sum_{m=2}^{l\geq m}4(n+2-2m)^2\right]\frac{\Delta_l}{k}$$
$$+ \sum_{l=1}^{n-1}\left[\frac{(n-1)(2n^2-7n+9)}{3} - \sum_{m=2}^{l\geq m}2(n+1-2m)^2\right]\varepsilon_{l,l+1}.$$

Solutions for cell numbering beginning with the drive cell numbered "1" and the other end cell numbered "N" are much more complicated and not as easy to display in a simple format. Solutions referenced to the drive cell can be determined as given above and then renormalized on the basis of the drive cell being $i_N = 1 + j0$.

Expressions for drive e_N in terms of i_1 or i_N are given below, eliminating smaller order terms:

$$e_N/i_1(\text{full}) = NR\left\{1 + \frac{2(N+1)(N-1)}{3}\alpha - \frac{(N-1)}{2N}k\right.$$
$$+ jkQ\left[\alpha - \frac{(N+1)(N-1)}{3k^2Q^2} - \frac{2}{k}(\Delta_1 + \cdots + \Delta_{N-2} + \Delta_{N-1} + \Delta_N)\right.$$
$$\left.\left. - (\varepsilon_{1,2} + \cdots + \varepsilon_{N-3,N-2} + \varepsilon_{N-2,N-1} + \varepsilon_{N-1,N})\right]\right\},$$

$$e_N/i_1(\text{half}) = (N-1)R\left\{1 + \frac{(2N^2-4N+3)}{3}\alpha - \frac{k}{2}\right.$$
$$+ jkQ\left[\alpha - \frac{(2N^2-4N+3)}{6k^2Q^2} - \frac{2}{k}\left(\frac{\Delta_1}{2} + \cdots + \Delta_{N-2} + \Delta_{N-1} + \frac{\Delta_N}{2}\right)\right.$$
$$\left.\left. - (\varepsilon_{1,2} + \cdots + \varepsilon_{N-3,N-2} + \varepsilon_{N-2,N-1} + \varepsilon_{N-1,N})\right]\right\},$$

$$e_N/i_N(\text{full}) = NR\Big\{1 - \frac{4(N-1)(N-0.5)}{3}\alpha - \frac{(N-1)}{2N}k + jkQ\Big[\alpha + \frac{2(N-1)(N-0.5)}{3k^2Q^2} - \frac{2}{k}(\Delta_1 + \cdots + \Delta_{N-2} + \Delta_{N-1} + \Delta_N) - (\varepsilon_{1,2} + \cdots + \varepsilon_{N-3,N-2} + \varepsilon_{N-2,N-1} + \varepsilon_{N-1,N})\Big]\Big\},$$

$$e_N/i_N(\text{half}) = (N-1)R\Big\{1 - \frac{4(N^2-2N+0.75)}{3}\alpha - \frac{k}{2} + jkQ\Big[\frac{\alpha + 2(N^2-2N+0.75)}{3k^2Q^2} - \frac{2}{k}\Big(\frac{\Delta_1}{2} + \cdots + \Delta_{N-2} + \Delta_{N-1} + \frac{\Delta_N}{2}\Big) - (\varepsilon_{1,2} + \cdots + \varepsilon_{N-3,N-2} + \varepsilon_{N-2,N-1} + \varepsilon_{N-1,N})\Big]\Big\},$$

from which it can be seen that resonance as seen from the drive cell or the other end cell is different. Differentiating the modulus of the above complex expressions with respect to α to find the minimum e_N/i value (resonance) yields the expressions for α_0 and α_{err} discussed in Sec. I. The definition for π-mode resonance of an errorless cavity with infinite Q is obvious. For a cavity with finite Q, resonance is defined when the expression for e_N/i is minimized, dependent on which cell is used to minimize this ratio (yielding the α term). As expected, phases from cell-to-cell are not identically π under these conditions.

For many applications Eq. (4) can be simplified to $i_n(\text{full})/(-1)^{n-1} \approx 1 + n(n-1)\alpha - j[n(n-1)/kQ]$. This simplification shows that the phase shift difference (from either the 0 or the π of a perfect lossless, errorless system) in the average on-axis fields from the end cell to the drive cell is given by $\Delta\phi_N(\text{full}) \cong -[N(N-1)/kQ](180/\pi)$ in degrees for small values. For example, a nine-cell cavity with $k = 0.01$ and a loaded $Q = 50\,000$ has a phase shift in the cell rf fields of $-8.3°$ from end to end; not inconsequential and a result not available from multicell mesh programs. Similar results can be obtained for a half-cell terminated cavity.

III. RESULTS OF CALCULATIONS FOR THE π-MODE

Extensive information for designing, constructing, and operating π-mode structures is available, especially for superconducting cavities [12–15]. This report provides additional information to assist early stages of π-mode cavity design and to provide an understanding of sensitivities to various cavity parameters. In particular, the following subsections provide information for cavity designers and builders, for interfaces with the cavity such as those needed by controls or rf engineers, and for operators of the cavities. The first topic discussed is off-resonance characteristics that show an interesting aspect when controlling cavities from end cells for errorless cavities. The second subsection, now allowing for errors in the cells, describes effects of the errors given by Eqs. (4) and (5), and provides expressions for the related π-mode frequency shifts. The third subsection uses the parameters discussed in subsection B with the results of cavity dimensions determined from SUPERFISH to provide tolerances for the cavity builder. All of these changes have impacts on the dispersion curves, impacts described in the subsection D. And finally, subsection E shows how to use the information from these dispersion curves to make estimates of field uniformity in the cavity, an important factor for efficient operation of the cavities.

A. Off-resonance field tilt

Differentiation of Eq. (4) with respect to α using the Eq. (2) relationship of f_π to α yields the following change in field amplitude for the π-mode: $\Delta i_n(\text{full})/(-1)^{n-1} \cong 2n(n-1)(1-k)\Delta f_\pi/kf_\pi$, an expression independent of Q that has been validated with LOOPER simulations. This expression defines relative cell-to-cell amplitude changes as a function of frequency shift Δf_π from resonance f_π. In some cases, cavity control may require accommodating this extra feature, in addition to the usual considerations for overall on-resonance control and for Lorentz force effects. For a five-cell cavity with a required field tolerance of $\pm 1/2\%$ and a k of 1%, the frequency tolerance $\Delta f_\pi/f_\pi$ is $\pm 1.25 \times 10^{-6}$ or ± 1 kHz at 800 MHz. The tilt in field changes direction, as expected, on either side of resonance as shown in a typical Q curve example (see Fig. 2), introducing an interesting aspect to some control algorithms. The example is for a 1%-coupled, 500 MHz, five-cell cavity with a loaded Q of 40 000. The peak in the Q curve as seen from the drive cell has a slightly different frequency than that as seen from the other end cell. An inverted quadratic function is the best fit to the entire Q curve using $\sigma^2/(\sigma^2 + \Delta f_\pi^2)$ with $\sigma^2 = (f_\pi/2Q)^2$ for the fit to the resonance power peak. These fits show that the drive cell resonance peak

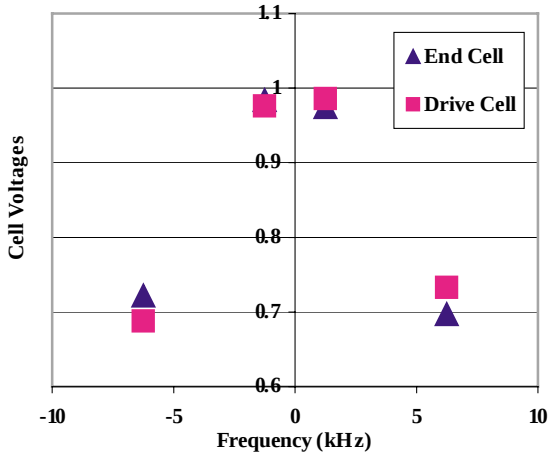

FIG. 2. (Color) Typical Q curves showing the field tilt difference between the end cell and drive cell fields as a function of frequency. Triangle and square points are for the end and drive cells respectively.

is $N(N-1)(1-k)f_\pi/2kQ^2$ distant from the other end cell resonance peak and has the same relative amplitude for an errorless cavity. For the example given above, the two resonance conditions would be 311 Hz apart.

B. Frequency and coupling errors in the cells

The above section gave field tilts for errorless cavities. With cell errors, field tilts can be much larger. Investigation of Eqs. (4) and (5) shows that an error ($\varepsilon_{n-1,n}$) in cell-to-cell coupling constant or an error (Δ_n) in frequency propagates throughout the entire cavity fields and is independent of Q. To minimize field errors, a frequency error in the nth cell requires adjacent cells to have opposite sign errors, one-half that of the nth value, i.e., $2\Delta_{n-1} = 2\Delta_{n+1} = -\Delta_n$. This correction yields field distributions almost as flat as if there were no errors in the cavity, except for cell n where a fractional field error $1/2$ that otherwise obtained is experienced. An exception to this tuning rule is for the end cells of a half-cell terminated cavity: to accommodate error Δ_1, $\Delta_1 = -\Delta_2 = 2\Delta_3$. Similar corrections are possible to accommodate coupling constant differences. Whatever coupling constant error exists, for fields almost as flat as those without errors the relationship $12\varepsilon_{1,2} = -4\varepsilon_{2,3} = 3\varepsilon_{3,4} = -3\varepsilon_{4,5} = 3\varepsilon_{5,6} = -3\varepsilon \cdots = \pm 4\varepsilon_{n-2,n-1} = \mp 12\varepsilon_{n-1,n}$ must be satisfied. One can achieve some flatness using $2\varepsilon_{n-1,n} = -\varepsilon_{n,n+1} = 2\varepsilon_{n+1,n+2}$; however, the local intercell field errors (about 0.6 of the coupling constant error) in the region (cells n and $n+1$) are a factor of 3 higher than that achieved with the more complex method.

Propagating through the entire cavity means, for example, a Δ/k or ε value of 0.01 yields field errors in a typical five-cell cavity ($k = 0.01$, loaded $Q = 60\,000$) along the length of from 2% up to 8% and from 1.4% up to 3%, respectively, depending on the location of the error. These values may not be as expected because there are two competing effects, with opposite signs, that cause field changes related to cell frequency or coupling constant errors. The first effect is related to the frequency shift from the error and affects all of the cells, whereas the second effect related to the actual error starts at the cell with the error and affects only the cells from it to the drive. As a consequence, there is a definite identification available to determine which cell has an error, even though at first glance the cavity symmetry would lead one to consider otherwise. This identification is possible because the drive cell breaks the symmetry. Another interesting effect is that having the drive in the center of a nine-cell cavity results in the cavity having properties similar to that of a five-cell cavity. Similarly, a seven-cell cavity driven in cell three demonstrates properties of a three-cell cavity for one part of the cavity and a five-cell cavity for the other part.

In addition to the introduced field errors, resonant frequency shifts determined from differentiating Eq. (2) and normalized for a single cell error are df_π (Hz) $= f_\pi$ (Hz)$k\varepsilon_{n,n-1}/[2(1-k)N]$ and df_π (Hz) $= (f_\pi/f_0) \times \Delta_N f_0$ (Hz)$/N$ for coupling constant and frequency errors, respectively. A simple sum determines the shift from multiple cell errors. The N term in the previous equations is $N-1$ for half-cell terminated cavities, and for this half-cell termination case the frequency shift is $1/2$ the value if the frequency error is in an end cell.

C. End cell tuning and coupling constants

Knowing the relationship between field tilt and cell errors discussed above gives tolerances for the errors. These tolerances can then be used to determine cell dimensional tolerances discussed in the following. First, however, SUPERFISH calculations are needed to determine parameters for end-cell tuning as a function of cell beta and beam-bore radius, the latter of which affects the cavity coupling constant. To obtain flat fields, as described above, the end cells of a full-cell terminated cavity need to be tuned to a different frequency than that of the main body of cells; higher in the case of the π-mode. One easy method to realize this requirement is to make the size of the end-bore radius larger than the beam-bore radius for at least one end-bore diameter in length away from the end cell. See Fig. 3 for a schematic showing the terms beam bore and end bore.

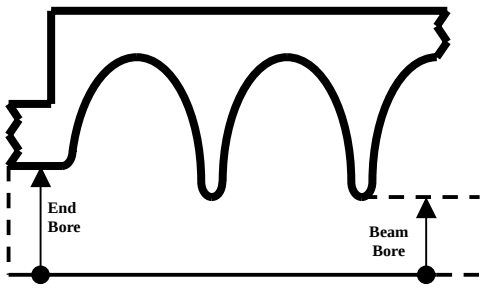

FIG. 3. Cavity schematic showing location for radii that determine end-bore and beam-bore sizes.

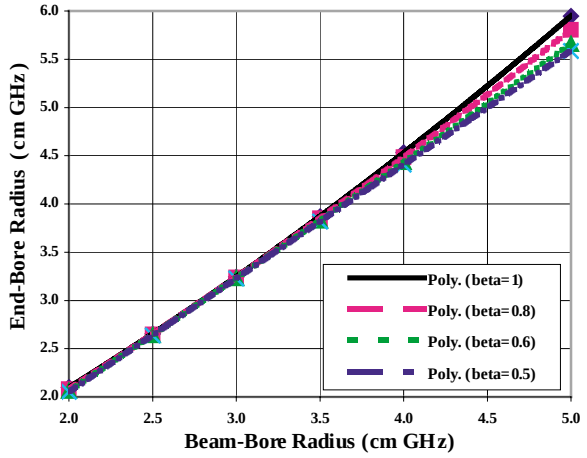

FIG. 4. (Color) Relationship between end-bore radius and the beam-bore radius. Units are given in cm GHz to enable design of different frequency cavities. Formulas for end-bore radius (R_E) in terms of beam-bore radius (R_B) are provided for different betas to assist with design considerations [($\beta = 1$, $R_E = 0.0676R_B^2 + 0.8103R_B + 0.2073$), ($\beta = 0.8$, $R_E = 0.041R_B^2 + 0.955R_B + 0.0052$), ($\beta = 0.6$, $R_E = 0.0143R_B^2 + 1.0998R_B - 0.1968$), ($\beta = 0.5$, $R_E = 0.001R_B^2 + 1.1722R_B - 0.2979$)].

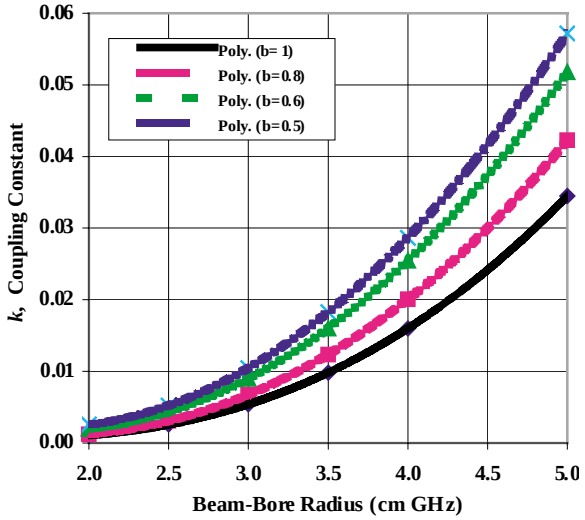

FIG. 5. (Color) Cavity coupling constant k as a function of beam-bore radius for different beta geometries. Formulas for k in terms of beam-bore radius (R_B) are provided for different betas to assist with design considerations [($\beta = 0.5$, $k = 0.000\,01R_B^3 + 0.005\,056R_B^2 - 0.017\,583R_B + 0.017\,442$), ($\beta = 0.6$, $k = 0.000\,078R_B^3 + 0.004\,007R_B^2 - 0.014\,495R_B + 0.014\,306$), ($\beta = 0.8$, $k = 0.000\,188R_B^3 + 0.002\,196R_B^2 - 0.009\,046R_B + 0.009\,025$), ($\beta = 1.0$, $k = 0.000\,265R_B^3 + 0.000\,767R_B^2 - 0.004\,567R_B + 0.005\,066$)].

Results described in the following were determined on the basis of multicell SUPERFISH calculations for elliptical-shaped cavities of different lengths having different beam-bore radii, with rounded noses in the cells forming the beam bores. Results in Fig. 4 are given in units of cm GHz, easing design for a particular frequency. For instance, a 3 cm beam-bore radius has a 3.25 cm end-bore radius at 1 GHz, while a 1 cm beam bore has a 1.08 cm end bore at 3 GHz. Formulas for end-bore radius versus beam-bore radius are given for different beta geometries that result in flat field distributions within a cavity for π-mode operation.

As described above, there are many advantages for a coupling constant k as high as possible. In the design process for a superconducting cavity, many variables are considered as described in Refs. [12,15]. In addition to important considerations of maximum magnetic field along the outer edge of the cell, maximum electric field on the cell surfaces and the ratio of peak surface electric field to on-axis accelerating field, circumstances exist under which it is possible to make allowance for having the coupling between cavities as high as possible. Figure 5 shows k as a function of beam-bore radius for different cell betas. The same data is displayed in another format in Fig. 6 for cases where this is a more appropriate format to assist parameter selection.

In order to maintain relative cell fields to within $1/2\%$, for the five-cell cavity described above ($1\%k$), coupling constant errors need to be within $1/6\%$ cell to cell. Figure 5 shows that tolerances at 1 GHz on beam bore vary from about 13×10^{-6} m for a 0.5 beta cell to 16×10^{-6} m for a 1.0 beta cell, tolerances which should not be difficult to attain. These tolerances would increase 50% if k were increased to 3%. Similarly, tolerances for Δ/k within $1/16\%$ (to maintain fields to within $1/2\%$) infer that the outer radius or the distance between adjacent cells (if these were the only impacting variables) must be within a 6.25×10^{-6} tolerance, or about 10^{-6} m for the radius at 1 GHz.

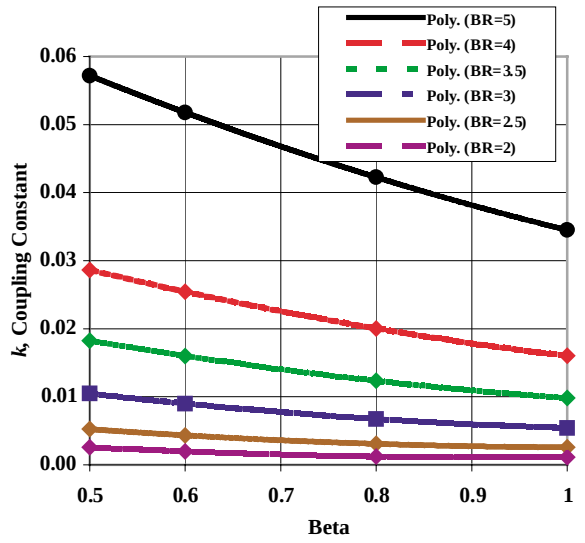

FIG. 6. (Color) Cavity coupling constant as a function of cavity beta for different beam-bore radii (BR) in cm GHz.

D. Dispersion curve characteristics with end cell tuning

In addition to the field tilts discussed above, detuning end cells of a full-cell terminated cavity has a significant effect on the passband or dispersion curve. Solving for the dispersion curve explicitly in terms of k, f_0, and the end cell frequency f_{end} is difficult because of the nature of determinant changes as a function of cell number. As expected, the equations and solution for a three-cell cavity are the typical doubly periodic format. Simple expressions for the modes of a four-cell cavity can be determined, as well as two modes of a five-cell system. All of the higher N cases are much more complicated. However, an inspection of the N cell dispersion curves, as shown in Fig. 7 for the same coupling constant at 500 MHz, shows that there is extreme sensitivity between the π-mode and the next nearest mode. The dispersion curve change is most noticeable between these two modes as the frequency of the end cell changes. The smaller the number of cells, the more exaggerated the curve becomes. The 0 to π dispersion curve for this set of parameters with no end cell tuning is shown for comparison purposes.

Figure 8 shows dispersion curves of a five-cell cavity for end-cell detuning sets with either the π-mode flattened (0 MHz) or the 0-mode flattened (0 MHz). Expected differences and the significant effect between the last two modes (π-mode flattening) or the first two modes (0-mode flattening) of the cavity are evident. Shown for each set are the dispersion curves for end cell detuning of ± 2 MHz that leads to nonflat fields. This changing dispersion curve pattern can be used to estimate or infer π-mode field distributions in a cavity by observing passband mode frequencies as a function of actions taken. The data required to make these inferences are provided in Figs. 9 and 10. Figure 9 provides parameters normalized to 500 MHz for straight-line fits that give coupling constant as a function of $[f(N) - f(N-1)]$, the frequency difference between the last mode (π-mode), and the mode closest to it. For instance, for a five-cell cavity, Fig. 9 yields $k = (500/f_0)\{(0.019\,075)[f(N) - f(N-1)] + (0.001\,290\,5)\}$, where f_0 is the cell frequency in MHz best determined from the first mode frequency, $f_0 = f(1)\sqrt{1 + k\cos[\pi/(N+1)]}$. For a $[f(N) - f(N-1)]$ difference of 2 MHz at 1000 MHz, k is 2.037%.

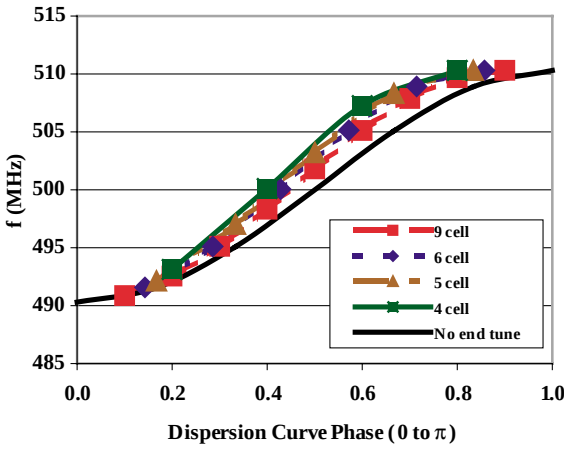

FIG. 7. (Color) Full-cell termination dispersion curves for different cell number cavities with 4% coupling at 500 MHz. End cells are tuned for a flat-field π-mode, except the one case showing the curve for all identical cells.

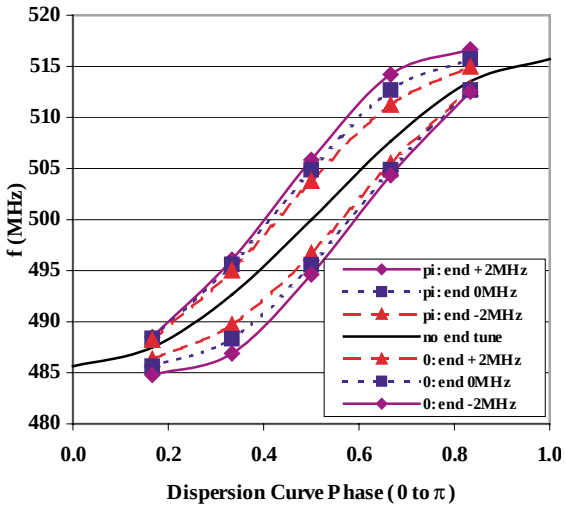

FIG. 8. (Color) Full-cell termination dispersion curves for π-mode cavity (upper three curves) and 0-mode cavity (lower three curves). End cells are detuned ± 2 MHz either side of the required end-cell frequency for achieving flat fields. The central curve is the dispersion curve with all cells identical.

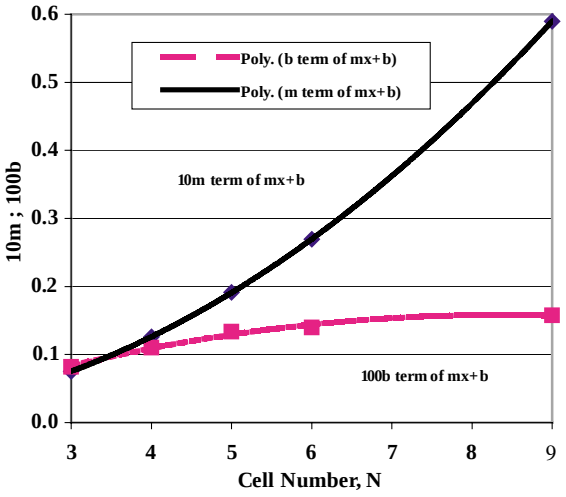

FIG. 9. (Color) Parameters "m" and "b" for cell numbers (N) from 3 to 9 used for the straight-line relationship $k = (500/f_0)\{m[f(N) - f(N-1)] + b\}$ to determine coupling constants on the basis of frequency separation where $f(n)$ is the nth mode frequency and f_0 is the cell frequency in MHz. Formulas that fit the data give $[(10m = 0.007N^2 + 0.0017N + 0.00725), \quad (100b = -0.00266N^2 + 0.0441\,N - 0.02495)]$.

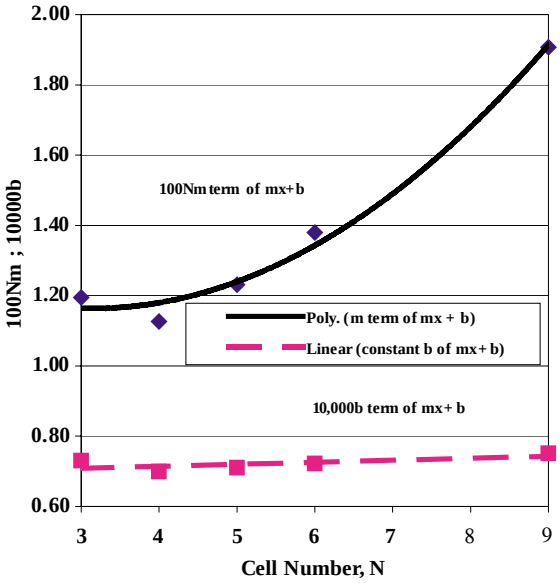

FIG. 10. (Color) Parameters "m" and "b" for cell numbers from 3 to 9 used for the straight-line relationship $k = (500/f_0)\{m[f(N-1) - f(1)] + b\}$ to determine coupling constants on the basis of frequency separation where $f(n)$ is the nth mode frequency and f_0 is the cell frequency in MHz. Formulas that fit the data give ($100Nm = 0.0218N^2 - 0.136N + 1.376$), ($10\,000b = 0.0058N + 0.6913$).

Similarly, Fig. 10 can be used to validate the calculated k value, or used with the above calculation to determine field differences from a fully flat field distribution as described below. Figure 10 provides the parameters normalized to 500 MHz for straight-line fits that give coupling constant as a function of $[f(N-1) - f(1)]$, the frequency difference between the second last mode and the first mode. For the same five-cell cavity, Fig. 10 yields $k = (500/f_0)\{(0.002\,482)[f(N-1) - f(1)] + (0.000\,0836\,3)\}$. For a $[f(N-1) - f(1)]$ difference of 14.8 MHz at 1000 MHz, k is 1.845%. Frequencies used in the above calculations were obtained from scaling five-cell Julich cavity results [16]. The passband frequencies from an errorless cavity would have provided identical k values when utilizing both methods. The ratio of these two values can be used to estimate field flatness, as long as results are within 10% of each other. In this case, fields should be flat to within 10.4% (2.037/1.845) with the center cell field being high, in agreement with the measured 7.2% high value for the central cell [16]. This agreement is reasonable because frequency differences were not only in the end cells, as an inspection of the relative field data infers.

E. Using dispersion curve characteristics for field pattern changes

The above subsection showed how to infer field flatness from relative measures of k. This process can be taken one step further to determine field flatness under changing conditions in a cavity. One of the difficulties in constructing and tuning a superconducting cavity is the fact that the on-axis field pattern is well known at room temperature, but is only assumed to remain the same at cryostat temperature. The following method suggests an indirect means for inferring field pattern change at cold temperature; based on the room temperature measurements, the mode spectra at cold temperature and a basic assumption. This method assumes that end cells behave in one manner because of connections to end-bore tubes and mechanical systems, while the middle cells behave in another manner because of their similarities to each other. This assumption can be checked in practice without having to go to very cold temperature. On this basis, the change in field pattern along the length of the cavity can be estimated by measuring the cavity mode spectra. The following gives an example of the method using Figs. 11–14. In the following, five-cell cavities and 500 MHz were used to demonstrate the suitability of the method.

From mode frequency measurements, an important dimensionless dispersion curve ratio is determined, $[f(N-1) - f(1)]/[f(N) - f(N-1)]$, using the frequency values associated with the measured on-axis field patterns. In the following this ratio is subscripted "meas." Similarly, the mode spectrum at the new operation point is used to determine a new ratio, subscripted as "temp." From these, the ratio $R1$ of $\{[f(N-1) - f(1)]/[f(N) - f(N-1)]\}_{\text{temp}}$ divided by $\{[f(N-1) - f(1)]/[f(N) - f(N-1)]\}_{\text{meas}}$ is calculated, a dimensionless and frequency independent function. This ratio, $R1$, was determined using LOOPER for many different system

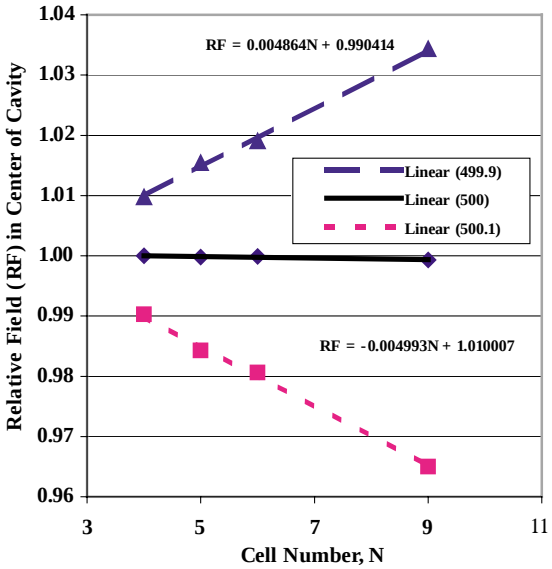

FIG. 11. (Color) Relative value of cavity midcell field to end-cell field as a function of cell number for different end-cell detuning of a 500 MHz cavity. Scaling for other frequency cavities is realized by multiplying the detuning scale, i.e., ± 0.4 MHz is used for 2 GHz cavities.

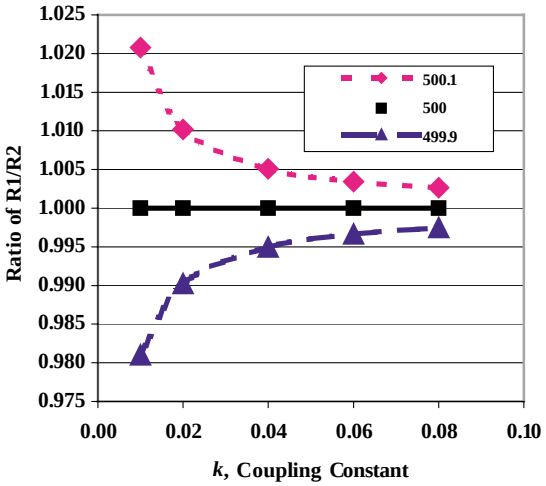

FIG. 12. (Color) Ratio $R1/R2$ as a function of coupling constant for different end-cell detuning of a 500 MHz cavity. Scaling for other frequency cavities is realized by multiplying the detuning scale, i.e., ± 0.4 MHz is used for 2 GHz cavities.

parameters $(N, k, Q, f_{\text{end}})$ with end cells detuned differently from the middle cells, relative to that required for a perfectly tuned π-mode cavity. The results were found to be independent of Q.

$E(\text{mid})$ in the following is the relative midcell field of an N cell cavity as compared to the end-cell field. With identical detuning of end cells (different from that of the middle cells), the field pattern has a symmetric shape about the middle of the cavity. $R2$ is defined as the ratio of $1/E(\text{mid})$ for an end-cell detuned cavity relative to $1/E(\text{mid})$ for a perfectly tuned π-mode cavity. Generally it has been found that $R1$ is almost identical to $R2$ unless the variations are very large ($>10\%$). Therefore, a measurement of $R1$ gives a good measure of the change to the cavity in $R2$, as long as the assumption that end cells change differently from the middle cells is valid. Figure 11 shows expected field changes in $E(\text{mid})$ versus cell number N for a case with a k of 4%. Similar curves showing linear behavior are found for different coupling constant values. This figure shows expected field changes varying from 1% to 3.5% when end cells are detuned up to ± 0.1 MHz relative to no change in midcells for a 500 MHz cavity. Everything is linear; a change of only ± 0.05 MHz results in $1/2$ the values shown. Figure 12 shows that the ratios $R1$ and $R2$ are almost equal over the range of interest. For 1% coupling, there is only a $\pm 2\%$ difference between the two ratios. Hence a 5% measured $R1$ ratio indicates a field pattern change of up to 4.9%. Another report, to be published soon, shows how to use actual mode spectra from an N cell π-mode cavity to determine which cells have errors, and the value of this error to be corrected, for either coupling or frequency errors.

Figures 13 and 14 show results similar to those for Figs. 11 and 12; however, for frequency detuning a factor of 20 larger (± 2 MHz). Although relative fields remain linear over the region shown in Fig. 13, the ratio $R1/R2$ varies much more. For instance, if $R1 = 0.9$ for a five-cell cavity with 2% coupling, then using Fig. 13 [initially assume $R2 = R1$ with $E(\text{mid})$ of 1.11] this indicates an almost -0.58 MHz end-cell detune. Figure 14 shows this -0.58 MHz detune to have a $R1/R2$ ratio of about 0.965, leading to a corrected value for $R2$ of 0.93 (0.9/0.965). Since $R2$ reflects changes in $1/E$, the E field has actually increased by 8%.

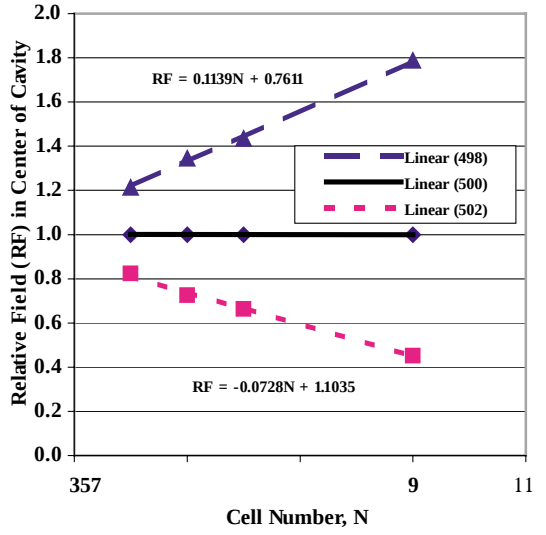

FIG. 13. (Color) Relative value of cavity midcell field to end-cell field as a function of cell number for different end-cell detuning of a 500 MHz cavity. Scaling for other frequency cavities is realized by multiplying the detuning scale, i.e., ± 8 MHz is used for 2 GHz cavities.

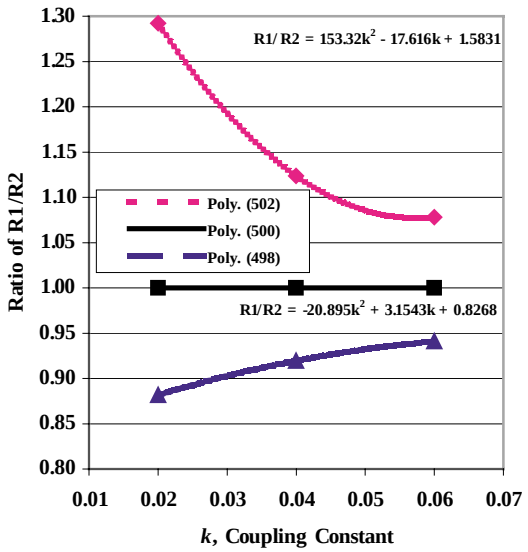

FIG. 14. (Color) Ratio $R1/R2$ as a function of coupling constant for different end-cell detuning of a 500 MHz cavity. Scaling for other frequency cavities is realized by multiplying the detuning scale, i.e., ± 8 MHz is used for 2 GHz cavities.

IV. CONCLUSIONS

A number of interesting trends have been determined for π-mode coupled cavities using coupled-circuit theory and solutions for various parametric variations. The analysis has shown advantages for coupling constants as high as possible ($k \geq 2\%$) within constraints of other parameters and conditions. The cell number in a cavity should be small ($N \leq 5$) to minimize error-related effects. A nine-cell cavity has two times the sensitivity as a five-cell cavity to errors and up to eight times for other operational issues. A method for inferring field flatness when a cavity is operated in an environment different from that when fields were measured has been developed. Experimental verification is needed before this method is fully accepted.

ACKNOWLEDGMENTS

The author thanks the Saclay Laboratory for providing an environment conducive to completing the work reported here. In particular, Jean-Louis Laclare, Jean-Michel Lagniel, and Henri Safa are thanked for interesting discussions on superconducting structure attributes and the associated beam dynamics possibilities. John Browne and his management team at Los Alamos are thanked for providing a unique opportunity for rekindling research interests. A special thanks to Jim Billen, Lloyd Young, Tom Wangler, and Frank Krawczyk for making a smooth transition possible, and for always being there no matter what my discussion topic covered. And finally, special thanks to Lorraine Stanford and Evelyn Schriber, for without their advice, support, and encouragement none of this would have been possible. This work was supported by the U.S. Department of Energy.

[1] J. H. Adlam and P. D. Dunn, Atomic Energy Research Establishment (AERE) Report No. GP/R 1539, 1954.

[2] P. D. Dunn, R. J. B. Hodden, and D. J. Thompson, Atomic Energy Research Establishment (AERE) Report No. GP/R 1962, 1956.

[3] P. D. Dunn, C. S. Sabel, and D. J. Thompson, Atomic Energy Research Establishment (AERE) Report No. GP/R 1966, 1956.

[4] P. D. Dunn and D. J. Thompson, Atomic Energy Research Establishment (AERE) Report No. GP/R 2000, 1957.

[5] D. E. Nagle and E. A. Knapp, in *Proceedings of the Conference on Proton Linear Accelerators* (Yale University Report No. TID-7691, 1963), p. 171.

[6] D. E. Nagel, in *Proceedings of the Conference on Proton Linear Accelerators Madison, Wisconsin* (Midwestern Universities Research Association Report No. MURA 714, 1964), p. 21.

[7] S. O. Schriber, in *Proceedings of the Proton Linear Accelerator Conference, Los Alamos, NM, 1972*, edited by K. H. Harper (Los Alamos National Laboratory Report No. LA-5115, 1972), p. 407.

[8] Helen Stokes Deaven and Kwok Chi Dominic Chan, Los Alamos National Laboratory Report No. LA-UR-90-1766, 1990; LAACG Online Software Compendium, http://laacg1.lanl.gov/laacg/componl.html.

[9] F. L. Krawczyk, J. H. Billen, R. D. Ryne, H. Takeda, and L. M. Young, in *Proceedings of the Particle Accelerator Conference, Dallas, Texas, 1995* (IEEE, Piscataway, NJ, 1996), p. 2306; http://laacg1.lanl.gov.

[10] J. H. Billen and L. M. Young, Los Alamos National Laboratory Report No. LA-UR-96-1834, 2001

[11] M. Clemens and T. Weiland, Journal of Electromagnetic Waves and Propagation/Progress in Electromagnetic Research (PIER) Monograph Series **32**, 65 (2001); http://www.cst.de/products/mafia/mafia.html.

[12] Jean-Luc Biarrotte, Saclay Report No. DAPNIA/SEA-00-01-T, 2001.

[13] F. L. Krawczyk, Los Alamos National Laboratory Report No. LA-UR-00-0015, 2001.

[14] D. Schrage *et al.*, in *Proceedings of the Seventh Workshop on RF Superconductivity, Saclay, France, 1995*, edited by B. Bonin (CEA/Saclay Report No. 96 080/1, 1996), p. 629.

[15] B. Aune *et al.*, Phys. Rev. ST Accel. Beams **3**, 092001 (2000).

[16] S. Martin and R. Stassen (private communication).